
This is an electronic reprint of the original article.

This reprint may differ from the original in pagination and typographic detail.

Ylivaara, Oili M.E.; Langner, Andreas; Ek, Satu; Malm, Jari; Julin, Jaakko; Laitinen, Mikko; Ali, Saima; Sintonen, Sakari; Lipsanen, Harri; Sajavaara, Timo; Puurunen, Riikka L.

Thermomechanical properties of aluminum oxide thin films made by atomic layer deposition

Published in:

Journal of Vacuum Science and Technology A: Vacuum, Surfaces and Films

DOI:

[10.1116/6.0002095](https://doi.org/10.1116/6.0002095)

Published: 01/12/2022

Document Version

Publisher's PDF, also known as Version of record

Published under the following license:

CC BY

Please cite the original version:

Ylivaara, O. M. E., Langner, A., Ek, S., Malm, J., Julin, J., Laitinen, M., Ali, S., Sintonen, S., Lipsanen, H., Sajavaara, T., & Puurunen, R. L. (2022). Thermomechanical properties of aluminum oxide thin films made by atomic layer deposition. *Journal of Vacuum Science and Technology A: Vacuum, Surfaces and Films*, 40(6), Article 062414. <https://doi.org/10.1116/6.0002095>

Thermomechanical properties of aluminum oxide thin films made by atomic layer deposition

Cite as: J. Vac. Sci. Technol. A **40**, 062414 (2022); <https://doi.org/10.1116/6.0002095>

Submitted: 20 July 2022 • Accepted: 24 October 2022 • Published Online: 18 November 2022

 Oili M. E. Ylivaara, Andreas Langner, Satu Ek, et al.

COLLECTIONS

Paper published as part of the special topic on [Atomic Layer Deposition \(ALD\)](#)



ARTICLES YOU MAY BE INTERESTED IN

[Role of ZnO and MgO interfaces on the growth and optoelectronic properties of atomic layer deposited \$\text{Zn}_{1-x}\text{Mg}_x\text{O}\$ films](#)

Journal of Vacuum Science & Technology A **40**, 062413 (2022); <https://doi.org/10.1116/6.0001925>


[Machine learning and atomic layer deposition: Predicting saturation times from reactor growth profiles using artificial neural networks](#)

Journal of Vacuum Science & Technology A **40**, 062408 (2022); <https://doi.org/10.1116/6.0001973>


[Area selective deposition of ruthenium on 3D structures](#)

Journal of Vacuum Science & Technology A **40**, 062412 (2022); <https://doi.org/10.1116/6.0002148>





HIDEN
ANALYTICAL



40 YEARS
1982 - 2022


Instruments for Advanced Science

- Knowledge,
- Experience,
- Expertise

Click to view our product catalogue


Contact Hiden Analytical for further details:
www.HidenAnalytical.com
info@hideninc.com

Gas Analysis




- ▶ dynamic measurement of reaction gas streams
- ▶ catalysis and thermal analysis
- ▶ molecular beam studies
- ▶ dissolved species probes
- ▶ fermentation, environmental and ecological studies

Surface Science




- ▶ UHVTPD
- ▶ SIMS
- ▶ end point detection in ion beam etch
- ▶ elemental imaging - surface mapping

Plasma Diagnostics



- ▶ plasma source characterization
- ▶ etch and deposition process reaction kinetic studies
- ▶ analysis of neutral and radical species

Vacuum Analysis



- ▶ partial pressure measurement and control of process gases
- ▶ reactive sputter process control
- ▶ vacuum diagnostics
- ▶ vacuum coating process monitoring

Thermomechanical properties of aluminum oxide thin films made by atomic layer deposition

Cite as: J. Vac. Sci. Technol. A 40, 062414 (2022); doi: 10.1116/6.0002095

Submitted: 20 July 2022 · Accepted: 24 October 2022 ·

Published Online: 18 November 2022



Oili M. E. Ylivaara,^{1,a)} Andreas Langner,¹ Satu Ek,² Jari Malm,³ Jaakko Julin,³ Mikko Laitinen,³ Saima Ali,⁴ Sakari Sintonen,⁴ Harri Lipsanen,⁴ Timo Sajavaara,³ and Riikka L. Puurunen^{1,5}

AFFILIATIONS

¹VTT Technical Research Centre of Finland, P.O. Box 1000, FI-02044 Espoo, Finland

²Picosun Oy, Tietotie 3, 02150 Espoo, Finland

³Department of Physics, University of Jyväskylä, P.O. Box 35, FI-40014 Jyväskylä, Finland

⁴Department of Electronics and Nanoengineering, Aalto University School of Electrical Engineering, P.O. Box 13500, FI-00076 Aalto, Finland

⁵Department of Chemical and Metallurgical Engineering, Aalto University School of Chemical Technology, P.O. Box 16200, FI-00076 Aalto, Finland

Note: This paper is part of the 2023 Special Topic Collection on Atomic Layer Deposition (ALD).

a) Author to whom correspondence should be addressed: oili.ylivaara@vtt.fi

ABSTRACT

In microelectromechanical system devices, thin films experience thermal processing at temperatures some cases exceeding the growth or deposition temperature of the film. In the case of the thin film grown by atomic layer deposition (ALD) at relatively low temperatures, post-ALD thermal processing or high device operation temperature might cause performance issues at device level or even device failure. In this work, residual stress and the role of intrinsic stress in ALD Al_2O_3 films grown from Me_3Al and H_2O , O_3 , or O_2 (plasma ALD) were studied via post-ALD thermal processing. Thermal expansion coefficient was determined using thermal cycling and the double substrate method. For some samples, post-ALD thermal annealing was done in nitrogen at 300, 450, 700, or 900 °C. Selected samples were also studied for crystallinity, composition, and optical properties. Samples that were thermally annealed at 900 °C had increased residual stress value (1400–1600 MPa) upon formation of denser Al_2O_3 phase. The thermal expansion coefficient varied somewhat between Al_2O_3 made using different oxygen precursors. For thermal- Al_2O_3 , intrinsic stress decreased with increasing growth temperature. ALD Al_2O_3 grown with plasma process had the lowest intrinsic stress. The results show that ALD Al_2O_3 grown at 200 and 300 °C is suitable for applications, where films are exposed to post-ALD thermal processing even at temperature of 700 °C without a major change in optical properties or residual stress.

© 2022 Author(s). All article content, except where otherwise noted, is licensed under a Creative Commons Attribution (CC BY) license (<http://creativecommons.org/licenses/by/4.0/>). <https://doi.org/10.1116/6.0002095>

I. INTRODUCTION

Thin films made by atomic layer deposition (ALD)^{1–9} are used as both passive and active layers, for example, in microelectromechanical system (MEMS) devices.^{10–12} ALD thin films are typically made at relatively low temperatures, below 400 °C, and after coating, these films might be exposed to subsequent thermal processing at temperatures higher than the actual growth temperature. In addition, the device operation temperatures might occasionally exceed the fabrication temperature depending on the environment of use. In these cases, thin films might experience measurable

permanent changes, for example, in the sense of the residual stress, composed of intrinsic and extrinsic stress components^{13–16} causing performance issues at device level or even device failure.

Even though residual stress data for ALD Al_2O_3 films are published on silicon^{11,17–44} and on polymers^{45–48} in a wide temperature range, it is unclear how a large quantity of the residual stress originates from extrinsic source (mainly thermal origin) and what is the role of intrinsic, growth-related stress in the film. The residual stress of thermal ALD Al_2O_3 is temperature dependent: residual stress decreases with increasing growth temperature.^{28,35}

From residual stress, we are able to differentiate the intrinsic stress part with thermal cycling, as the residual stress measured at the growth temperature can be assumed to be equal to intrinsic stress.⁴⁹ By thermal cycling, the coefficient of the thermal expansion (CTE) of the thin film can be extracted using the so-called double substrate method.^{50,51} In the double substrate method, the studied material is grown on two substrates with different CTE values. When the double substrate method is used, the coefficient of the thermal expansion of the film, α_f , is calculated as follows:⁵⁰

$$\alpha_f = \frac{\alpha_{s2} \frac{\sigma_{f1}(T)}{\Delta T} - \alpha_{s1} \frac{\sigma_{f2}(T)}{\Delta T}}{\frac{\sigma_{f1}(T)}{\Delta T} - \frac{\sigma_{f2}(T)}{\Delta T}},$$

where σ_{f1} is the residual stress of the first film on a first substrate, σ_{f2} is the residual stress of the second film on a second substrate, α_{s1} is the CTE of the first substrate, α_{s2} is the CTE of the second substrate, and ΔT is the selected temperature range for which the measured stress-temperature slopes $\frac{\sigma_f(T)}{\Delta T}$ should be linear.

The residual stress and mechanical properties of ALD thin films can be tuned by changing the growth temperature by adding inter-layers into the material or by using laminated thin films.^{12,34,44,52,53} Post-ALD thermal processing affects residual stress via changes in film morphology, density, or impurity content.⁵² In some cases, the post-ALD thermal processing might cause additional problems, for example, blistering due to outgassing of trapped hydrogen,^{38,54–58} especially known to appear with pinhole-free ALD Al_2O_3 films, and also delamination problems due to the CTE mismatch between the substrate and the film. Crystallization of ALD Al_2O_3 requires high annealing temperatures, and it has been reported to start at around 800 °C,^{17,18,23,59,60} and it is seen as a rise in residual stress upon volume change caused by crystallization. Crystallization has been reported to increase also elastic modulus and hardness^{60–62} and to alter electric breakdown properties.⁶³

The purpose of this work was to study the role of the ALD growth temperature, precursor combination, and post-ALD thermal processing to residual stress and optical properties of the ALD Al_2O_3 thin films. Studied material was ALD Al_2O_3 grown using Me_3Al as a metal precursor and in thermal ALD process either H_2O or O_3 or in plasma-assisted process O_2 as the oxygen source. Influence of post-ALD thermal processing to ALD thin film was tested via thermal annealing and thermal cycling. The thermal cycling revealed the role of intrinsic stress in the film, and the double substrate method was used to determine the CTE for ALD Al_2O_3 .

II. MATERIALS AND METHODS

Thermal ALD Al_2O_3 thin films were grown in Picosun® SUNALE R-150 reactor with three reactant lines from Me_3Al (trimethylaluminum, CAS No.: 75-24-1, electronic grade) and de-ionized H_2O (resistivity of 18.2 MΩ cm) at a temperature range of 110–300 °C. Pulse and purge times were 0.1 and 4.0 s, respectively, for both Me_3Al and H_2O . There was a constant 200 SCCM nitrogen 6.0 flow through the reactant lines. At temperature range from 30 to 110 °C, thermal Al_2O_3 films from Me_3Al (electronic

grade) and H_2O were grown in Beneq TFS 200 reactor at University of Jyväskylä. For these samples, the pulse lengths for Me_3Al and H_2O were 0.15 s through the temperature range. The purge length was varied, being 10.0, 7.0, 5.0, 4.0, and 2.0 s for Me_3Al and 30.0, 20.0, 10.0, 5.0, and 3.0 s for H_2O at temperatures 30, 50, 70, 90, and 110 °C, respectively. Some thermal Al_2O_3 samples were grown from Me_3Al (Strem chemicals >98%, further purified by Volatec) and O_3 ($\geq 99.9999\%$, CAS No.: 10028-15-6) as an oxygen source in the Picosun™ R-200 standard ALD equipment at the Picosun facilities. The plasma ALD Al_2O_3 from Me_3Al and O_2 (CAS No. 7782-44-7) was grown using Picosun™ R-200 Advanced with remote plasma ALD system at the Picosun facilities. Plasma power was fixed to 2.5 kW, while the O_2 flow was 90 SCCM and the Ar flow was 40 SCCM. ALD growth details are presented in Table I. In all samples, targeted film thickness was 100 nm.

ALD thin films were grown on 150 mm (100) double side polished silicon wafers with thickness of $380 \pm 5 \mu\text{m}$. Silicon wafers were RCA-cleaned, and some wafers were thermally annealed at 950 °C for 30 min in nitrogen prior to ALD. The purpose with pre-ALD thermal annealing was to prevent possible blistering occurring in the films during post-ALD thermal processing. Selected samples were post-ALD thermal annealed at 300, 450, 700, or 900 °C for 30 min using the 1000 SCCM nitrogen flow. The annealing furnace was ATV Technologie GmbH PEO-603.

Optical characterization on full range (from UV to NIR) was done using FilmTek4000 spectroscopic reflectometry. Furthermore, the samples were analyzed with x-ray reflectivity (XRR), x-ray diffractivity (XRD),²⁸ and time-of-flight elastic recoil detection analysis (TOF-ERDA)^{64,65} for density, crystalline structure, and impurities, respectively. The wafer curvature measurements were done on blank silicon wafers before ALD, after ALD, and after post-ALD thermal annealing using the Toho Technology FLX 2320-S laser-based wafer curvature measurement tool. The residual stress was calculated via Stoney's equation. The wafer curvature was measured in two directions, in parallel and perpendicular to the wafer flat. The residual stress values given here are average values from these two measurements and are given with maximum measurement uncertainty.²⁸

Some wafers were thermally cycled from room temperature up to 500 °C and back to room temperature with *in situ* wafer curvature measurement using Toho Technology FLX 2320-S. As this measurement is destructive, the measurement was done only in parallel to the wafer flat, along so-called x-axis. The wafer was held at maximum temperature, 500 °C for 1 min before cooling started. The heating ramp rate was 10 °C/min. Thermal cycling was repeated non-stop maximum of three times. During thermal cycling, the wafers were under continuous nitrogen flow, but the atmosphere was not completely oxygen free.

The thermal expansion coefficient of ALD Al_2O_3 was evaluated using the double substrate method. Silicon (100) and single-crystal sapphire were used as a substrate material. Single side polished sapphire wafers (100 mm, $526 \pm 9 \mu\text{m}$ from Kyocera) were cleaned with SC1 ($\text{NH}_3:\text{H}_2\text{O}:\text{H}_2\text{O}_2$ 1:5:1, 65 °C, 10 min) followed by SC2 ($\text{HCl}:\text{H}_2\text{O}:\text{H}_2\text{O}_2$ 1:5:1, 60 °C, 10 min) prior to the ALD process. The ALD process on sapphire was identical compared to coatings made on silicon wafers. Backsides of the wafers were protected during the ALD growth using another wafer, rough side against the backside. The backside growth was larger for 100 mm sapphire wafers about

TABLE I. Growth parameters and characterization results for ALD Al_2O_3 grown from Me_3Al and H_2O before and after post-ALD thermal annealing at 300, 450, 700, and 900 °C and for as-grown ALD Al_2O_3 from Me_3Al and O_2 plasma. Residual stress values are presented with maximum measurement uncertainty. All other characterization results are presented with standard deviation of the measurement.

	ALD growth				Residual stress		Post-ALD annealing											
	Temp °C	Cycles	Thickness		On silicon MPa	Temp °C	Thickness		n @ 635 nm	Density g/cm ³	Roughness nm	Residual stress		Hydrogen at. %	Carbon at. %	O/Al		
			nm	±			Nm	±				MPa	±					
Me ₃ Al-H ₂ O	30	1316	101.0	0.5	−366	18	—	—	—	2.44	0.6	—	—	30.00	±2.00	2.60	±0.20	2.07
	50	1266	98.2	0.2	229	14	—	—	—	2.56	0.7	—	—	23.00	±1.00	2.20	±0.10	1.86
	70	1205	97.8	0.1	412	18	—	—	—	2.65	0.7	—	—	16.80	±0.50	1.60	±0.10	1.71
	90	1149	97.5	0.1	482	23	—	—	—	2.70	0.7	—	—	13.80	±0.50	1.30	±0.10	1.70
	110	1087	98.5	0.2	490	20	—	—	—	2.80	0.7	—	—	11.60	±0.50	1.20	±0.10	1.62
	110	1283	97.8	3.2	472	36	—	V	1.61	2.80	0.7	—	—	11.30	±0.20	0.90	±0.06	1.65
	110	1283	97.3	3.3	478	37	300	96.2	3.4	2.85	0.7	414	34	10.60	±0.20	0.89	±0.06	1.67
	110	1283	97.2	3.3	478	36	450	94.5	3.2	2.80	0.7	549	43	8.00	±0.20	0.88	±0.05	1.62
	110	1283	97.8	3.2	477	37	900	80.6	3.8	3.45	1.0	1591	134	0.44	±0.04	0.96	±0.06	1.53
	200	1037	99.8	2.2	318	25	—	—	1.64	—	0.8	—	—	2.70	±0.11	0.19	±0.03	1.58
Me ₃ Al-O ₃	200	1037	99.2	2.0	322	23	700	97.8	2.1	1.64	—	391	28	0.78	±0.06	0.25	±0.03	1.52
	300	1109	109.0	1.4	220	15	—	—	1.65	3.10	0.6	—	—	1.19	±0.07	0.08	±0.02	1.56
	300	1109	109.1	1.5	214	15	300	109.3	1.5	3.05	0.6	220	15	1.07	±0.07	0.09	±0.02	1.55
	300	1109	109.0	1.4	229	16	450	109.0	1.4	3.05	0.6	261	17	1.06	±0.07	0.11	±0.02	1.56
	300	1109	109.9	1.1	222	15	700	108.7	1.3	3.05	0.6	336	21	0.26	±0.03	0.09	±0.02	1.55
	300	1109	109.6	1.2	215	15	900	99.8	1.3	3.60	1.1	1431	65	0.11	±0.02	0.08	±0.02	1.52
	110	1110	94.2	1.7	401	25	—	—	—	2.60	0.7	—	—	11.00	±1.50	6.30	±0.50	2.03
	200	1235	103.0	2.1	548	36	—	—	—	2.90	0.8	—	—	3.30	±0.40	1.90	±0.20	1.69
	300	1150	99.4	1.0	274	17	—	—	—	3.05	0.5	—	—	0.50	±0.10	0.23	±0.05	1.55
	Me ₃ Al-O ₂ ^a	110	1090	109.6	4.4	564	45	—	—	—	2.80	1.0	—	—	6.70	±0.20	2.60	±0.20
200		1168	109.7	3.5	424	33	—	—	—	3.00	0.9	—	—	2.10	±0.20	0.63	±0.10	1.56
300		1142	95.9	2.2	191	17	—	—	—	3.05	0.7	—	—	—	—	—	—	—

^a O_2 plasma.

5–10 mm compared to the backside growth of 150 mm silicon wafers, giving a somewhat larger measurement uncertainty for sapphire wafers. The magnitude of the backside growth to residual stress was not analyzed on sapphire wafers. After the ALD growth, the sapphire wafers were thermally cycled with the same equipment and parameters as the silicon wafers. Film thickness was assumed to be the same on silicon and sapphire. The thermal expansion coefficient of 3.08 and 5.37 ppm/°C was used for silicon⁵⁰ and sapphire,⁶⁶ respectively, at temperature range from about room temperature (RT) to 180 °C. And at temperature range from about RT to 500 °C, CTE values of 3.45 and 7.0 ppm/°C were used for silicon²⁵ and sapphire,⁶⁶ respectively. Different substrate CTE values were used at different temperature ranges because substrate CTE varies with temperature.⁵⁰ Temperature range from RT to 500 °C was selected because most ALD Al₂O₃ CTE values^{25,26} are published on this temperature range.

III. RESULTS AND DISCUSSIONS

ALD Al₂O₃ thin films were characterized for thickness, refractive index, density, and residual stress after ALD and after post-ALD thermal annealing; results are presented in Table I. For as-grown samples made from Me₃Al and H₂O, there was a positive correlation between growth temperature (temperature from 30 to 300 °C) and film density. The density increased with increasing ALD temperature. Surface roughness measured by XRR was independent of the ALD temperature. Low-temperature sample grown at 30 °C had high amount of hydrogen, about 30 at. %. The amount of hydrogen decreased with increasing ALD temperature. The amount of the residual carbon decreased with increasing ALD temperature from 2.6 to 0.08 at. %. There was a linear negative correlation between hydrogen in the film and the film density and between the residual carbon and the film density. Low-temperature samples grown at 30–110 °C had small amount of residual chlorine (not included in the Table I) from the reactor, amount being highest at 0.16 ± 0.03 at. % at 110 °C. Film grown at 30 °C was

oxygen-rich O/Al ratio being 2.07. High-temperature films had O/Al ratio near stoichiometric Al₂O₃.

For different ALD Al₂O₃ precursor combinations, impurity content (Table I) decreased with increasing ALD temperature. Plasma ALD Al₂O₃ from Me₃Al-O₂ had the low hydrogen content for sample processed at 110 °C of 6.7 at. % compared to about 11 at. % for thermal ALD processes. Thermal Al₂O₃ from Me₃Al-O₃ had high, 6.3 at. % carbon concentration for sample grown at 110 °C, at this temperature also density was lower compared to samples made using other oxygen sources. Me₃Al-O₂ and Me₃Al-O₃ were oxygen rich grown at low temperature, at 110 °C. Samples grown at higher temperatures were closer to stoichiometric Al₂O₃. In every case, density increased with increasing ALD temperature. All as-grown samples were amorphous in XRD.

Thickness decrease was observed upon post-ALD thermal annealing for Me₃Al-H₂O samples grown at 110, 200, and 300 °C. Notable thickness change was observed for samples annealed at highest temperature at 900 °C, where also highest values for refractive index (1.71 nm) and density (3.60 g/cm³) were measured. Thickness reduction with increasing post-ALD thermal annealing temperature was due to film densification; thickness reduction upon annealing has been previously reported by several sources.^{17,67–69} Upon annealing, the hydrogen content decreased with increasing annealing temperature, being at lowest value after annealing at 900 °C. In carbon content, no change upon annealing was detected. The O/Al ratio decreased about 7% for sample grown at 110 °C and annealed at 900 °C.

Refractive index and extinction coefficients were measured as a function of wavelength for as-grown and post-ALD thermally annealed Me₃Al-H₂O samples. The sample grown at 110 °C had lowest refractive index values through the wavelength range from 190 to 1650 nm [Fig. 1(a)]. In refractive index, no major changes were measured after thermal annealing up to 700 °C. Thermal annealing at 900 °C caused a notable change in refractive index for samples grown at 110 and 300 °C. In the extinction coefficient, however, the only nonzero value throughout the wavelength range

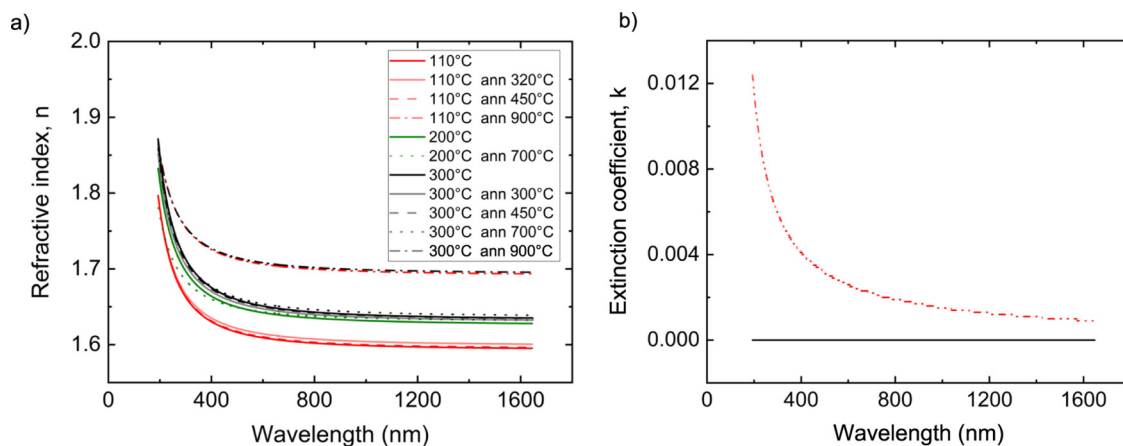


FIG. 1. Refractive index spectra of ALD Al₂O₃ coatings on silicon after the growth and after thermal annealing (a), and extinction coefficient, (b) as a function of wavelength from about 190 to 1650 nm. In (b), all curves except 110 °C sample annealed at 900 °C overlap at zero.

was measured for the sample grown at 110 °C and thermally annealed at 900 °C, and all other samples were nonabsorptive [Fig. 1(b)]; this was the only sample where blistering was detected.

Residual stress results for as-grown Al_2O_3 samples and samples after post-ALD thermal annealing are presented in Table I. For thermal Al_2O_3 made from $\text{Me}_3\text{Al-H}_2\text{O}$, in a temperature range from 90 to 300 °C, there was a linear negative correlation (−0.99) between ALD growth temperature and residual stress. The residual stress decreased with increasing ALD temperature. This was in line with previously published results.^{28,35} The residual stress of the samples grown at temperatures from 30 to 70 °C showed linear positive correlation (0.96) with increasing ALD temperature. The reason for this behavior is unknown. In this temperature range, from 30 to 70 °C, residual stress had linear positive correlation with film density (0.98) and linear negative correlation with O/Al ratio (−0.98) and impurity content of the film (−0.97 for H and −0.92 for C). For plasma- Al_2O_3 from $\text{Me}_3\text{Al-O}_2$, the residual stress decreased linearly with increasing ALD growth temperature (correlation of −0.99). For thermal $\text{Me}_3\text{Al-O}_3$ process, there was no linear correlation between the residual stress and ALD growth temperature detected (correlation of −0.49). The residual stress result for repeated thermal $\text{Me}_3\text{Al-O}_3$ sample was alike.

For samples grown at 300 °C, highest residual stress was measured for thermal- O_3 -based Al_2O_3 process, and residual stress value for the film was 274 ± 17 MPa compared to residual stress of a thermal H_2O -based material of about 220 MPa and a plasma- O_2 -based material of 190 MPa. Comparison to published residual stress values for films made by plasma-ALD from Me_3Al and O_2 gives no comprehensive image of the residual stress as published residual stress values^{25,26,35,42} vary from compressive to tensile even at the same ALD temperature. High dispersion of published residual stress values in plasma ALD Al_2O_3 is most probably related to many variables in plasma processes. For the thermal $\text{Me}_3\text{Al-O}_3$ process, only a single publication covering residual stress was found.¹⁸

The residual stress (Table I) increased due to post-ALD thermal annealing already at temperatures of 450 °C; a high-rise was observed on samples annealed at 900 °C. In literature up to 2000 MPa, tensile residual stress has been measured for ALD Al_2O_3 film annealed at 850 °C.²³ Here, maximum values of about 1400–1600 MPa were measured upon thermal annealing at 900 °C. At this temperature, high values have been measured also for elastic modulus and hardness,⁶¹ and ALD Al_2O_3 has been reported to be polycrystalline, depending on film thickness, containing islands with mixture of different crystalline phases surrounded by an amorphous film.^{17,18,70} Cubic γ - Al_2O_3 has been reported at 950 °C,⁷⁰ and crystallization to alpha- Al_2O_3 requires annealing at 1150 °C.⁷¹

Thermal cycling results (numerical data are given in the supplementary material⁷³) of ALD Al_2O_3 on silicon, residual stress as a function of temperature, are presented in Fig. 2 for thermal H_2O and O_3 and plasma- O_2 -based samples. There was no difference in thermal behavior between $\text{Me}_3\text{Al-H}_2\text{O}$ samples that were preannealed before ALD growth or samples without preannealing. Only preannealed $\text{Me}_3\text{Al-H}_2\text{O}$ sample results are presented here and data for samples without preanneal are presented in the supplementary material.⁷³ The sample grown at 110 °C was the only sample where irreversible changes in the

stress-temperature curve were observed during the first heating cycle. Samples with other precursor combination and growth temperature had a reversible stress-temperature curve, indicating good stability of the material over the used temperature range. In each case, the stress values headed toward more compressive values with increasing annealing temperature, meaning that Al_2O_3 films have larger CTE than the silicon substrate. These results are in line with published ALD Al_2O_3 thermal cycling results on silicon^{21,22,25} although for much thinner films opposite results have been published.¹⁸

Sapphire was used as an alternative substrate material. Figure 3 presents stress-temperature curves for Al_2O_3 on sapphire wafers grown using different oxygen precursors H_2O , O_3 , and O_2 . The curvature data as a function of temperature were more scattered on sapphire compared to what were measured on silicon. All the samples showed a reversible stress-temperature curve. Although large residual stress values were observed for plasma $\text{Me}_3\text{Al-O}_2$ and thermal $\text{Me}_3\text{Al-H}_2\text{O}$ samples at thermal cycling temperatures close to 500 °C, no permanent changes in the residual stress were observed when samples were cooled back to room temperature. Upon annealing, the residual stress of Al_2O_3 on sapphire shifted toward more tensile values indicating higher CTE of the sapphire substrate compared to the CTE of the film. We did not define thermal stress values for Al_2O_3 on sapphire as there was large scatter between the results of consecutive measurements; this was also the reason why actual residual stress value were not given for Al_2O_3 on sapphire.

Table II presents the CTE values calculated for the ALD Al_2O_3 films using the double substrate method. The CTE values were determined from $\frac{\sigma_f(T)}{\Delta T}$ slopes (result from linear fitting⁷²) on a temperature range from about RT to 180 °C and on some samples on a temperature range from RT to 500 °C. There was no clear difference between the CTE values in thermal processes using either O_3 or H_2O as the oxygen source, nor between thermal and plasma processes on a temperature range of RT to 180 °C. The standard error from linear fitting on a sapphire substrate was in such a large role that no general conclusions could be made on the CTE value as a function of the ALD growth temperature. Moreover, because of the large standard error, the CTE value calculated for $\text{Me}_3\text{Al-H}_2\text{O}$ grown at 110 °C should not be considered reliable. On a broader temperature range, from RT to 500 °C, thermal $\text{Me}_3\text{Al-O}_3$ had largest CTE value, and difference to CTE value of thermal $\text{Me}_3\text{Al-H}_2\text{O}$ was significant.

The CTE values presented here are approximately in line with published CTE values.^{21,25,26,37} In literature decreasing CTE as a function of increasing ALD temperature has been reported for ALD Al_2O_3 .^{25,26} Here, the magnitude of standard error in the linear fit was large for sapphire wafers causing uncertainty in CTE determination and no such conclusion could be made.

Intrinsic stress (Table II) defined at annealing temperature corresponding to the actual film growth temperature had a linear negative dependence to growth temperature (correlation −0.99); intrinsic stress decreased with increasing ALD temperature. Decreasing intrinsic stress with increasing ALD temperature is in line with theoretical calculations presented earlier.²⁸ Intrinsic stress varied for samples made using different oxygen precursors and

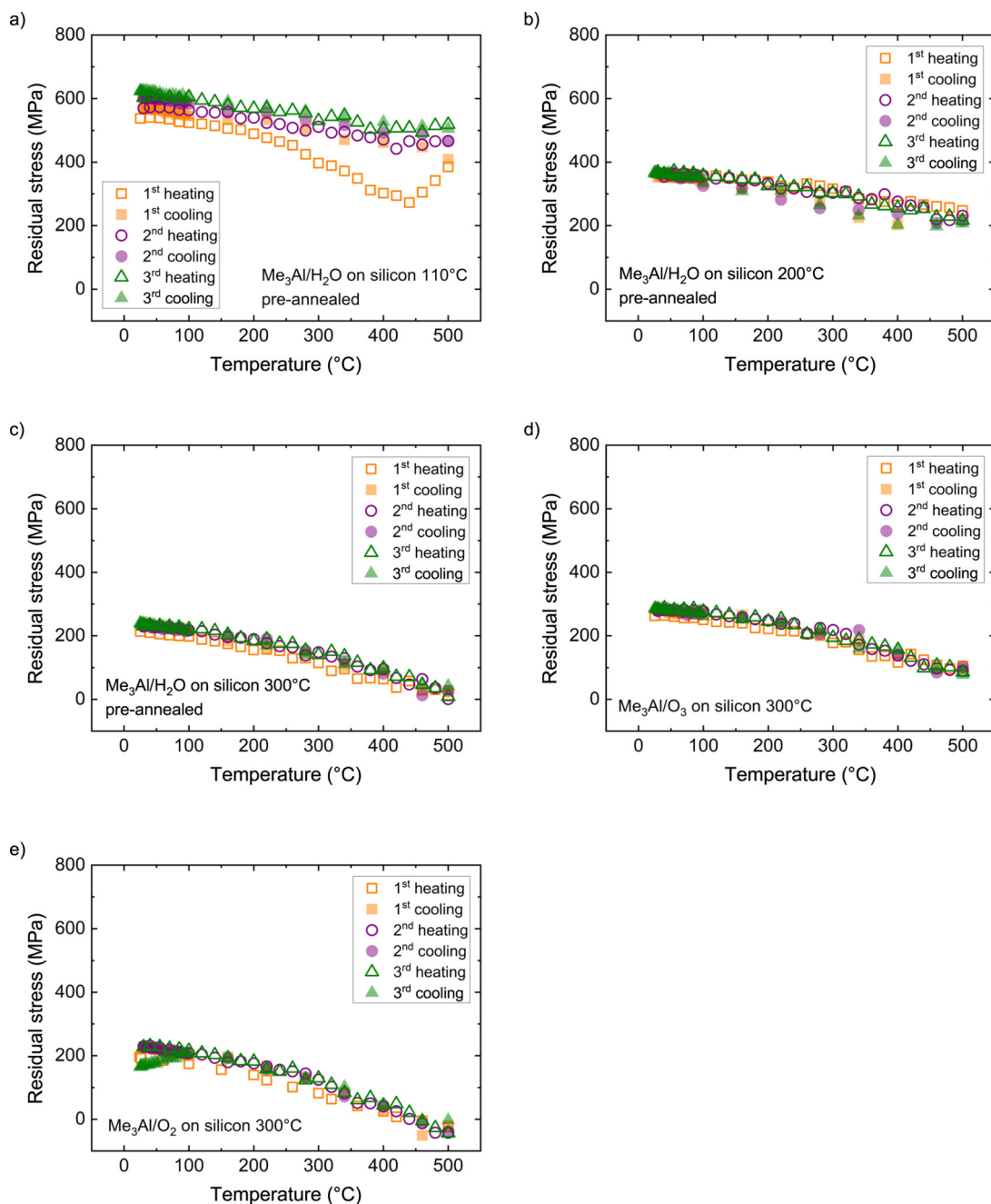


FIG. 2. Residual stress as a function of thermal cycling temperature for ALD Al_2O_3 on silicon from Me_3Al and H_2O grown at (a) 110, (b) 200, and (c) 300 °C and (d) from Me_3Al and O_3 grown at 300 °C and (e) Me_3Al and O_2 (plasma) grown at 300 °C.

thermal/plasma processes: for the plasma- O_2 process, about 44% of the stress was from intrinsic origin, while for the thermal H_2O -based material, about 55% of the stress was from intrinsic origin. As intrinsic stress was examined as a function of growth

temperature, we see that intrinsic stress was in major role, as around 95% of the stress was from intrinsic origin for films grown at 110 and 200 °C and this is most probably related to higher impurity content of the film.

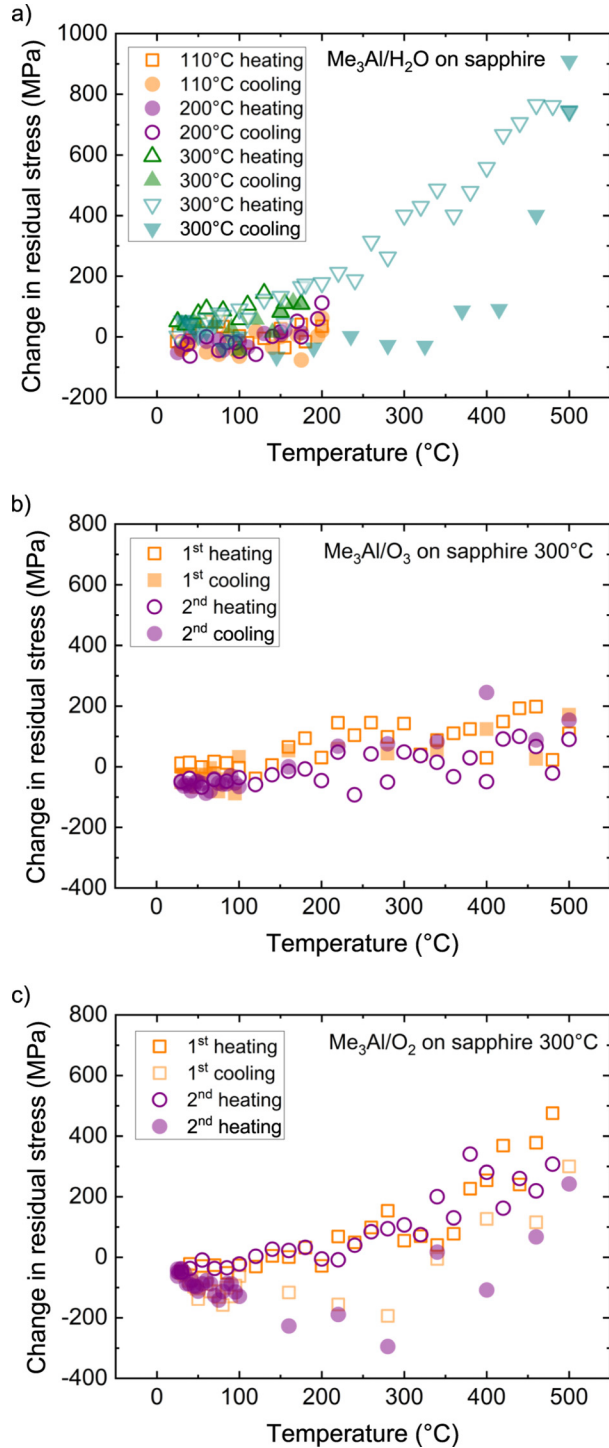


FIG. 3. Change in residual stress as a function of thermal cycling temperature from about room temperature up to 500 °C for ALD Al_2O_3 on sapphire from (a) Me_3Al and H_2O grown at 110, 200, and 300 °C, (b) Me_3Al and O_3 grown at 300 °C, and (c) Me_3Al and O_2 (plasma) grown at 300 °C.

TABLE II. Slopes $\Delta\sigma/\Delta T$ measured for ALD Al_2O_3 from different precursor combinations on silicon and on sapphire wafers. Temperature range was from about RT to 180 °C and for samples grown at 300 °C from RT to 500 °C. Intrinsic stress was approximated on thin films on silicon from the stress-temperature curve during first heat cycling at temperature corresponding to actual growth temperature. Thermal expansion coefficient values were calculated from $\Delta\sigma/\Delta T$ values using the double substrate method.

Temperature range	Precursors	ALD temperature (°C)	Sapphire		Silicon		Thermal expansion coefficient	
			Slope (MPa/°C)	Standard error ±	Slope (MPa/°C)	Standard error ±	Intrinsic stress MPa	ppm/°C
RT–180 °C	$\text{Me}_3\text{Al} + \text{H}_2\text{O}$	110	−0.1203	0.1756	−0.2600	0.0183	520	7.340
		200	0.3862	0.1202	−0.1108	0.0223	340	3.590
		300	0.4758	0.1484	−0.2974	0.0177	115	3.960
RT - 500 °C	$\text{Me}_3\text{Al} + \text{O}_3$	300	0.4530	0.1781	−0.2335	0.0218	180	3.860
		300	0.4227	0.1077	−0.3136	0.0134	80	4.055
	$\text{Me}_3\text{Al} + \text{O}_2$ plasma	300	1.7536	0.0844	−0.4388	0.0135	—	3.840
		300	0.3230	0.0613	−0.3791	0.0149	—	4.480
	$\text{Me}_3\text{Al} + \text{O}_2$ plasma	300	1.0450	0.1031	−0.4802	0.0153	—	4.055

IV. CONCLUSIONS

The thermal behavior of ALD Al_2O_3 grown from trimethylaluminum with different oxygen precursors (H_2O , O_3 , and O_2 plasma) was studied via post-ALD thermal annealing and thermal cycling. The thermal stability of the films grown at 200 and 300 °C was good, as no permanent changes were observed in the residual stress, also the refractive index and extinction coefficient remained stable upon thermal annealing at 700 °C. Samples annealed at 900 °C had increased residual stress and clear rise in the refractive index [and in the extinction coefficient (sample grown at 110 °C)]. The thermal expansion coefficient varied somewhat between different oxygen precursors in the temperature range from about RT to 500 °C. At narrower temperature range from about RT to 180 °C, there was no statistical difference in the thermal expansion coefficients between different ALD temperatures or oxygen precursors detected. Intrinsic stress decreased with increasing growth temperature. Comparison between Al_2O_3 samples grown at 300 °C using different oxygen precursors revealed clear differences in intrinsic stress; lowest intrinsic stress was with ALD Al_2O_3 grown with O_2 plasma. The results show that ALD Al_2O_3 is suitable for applications where the films are exposed to moderate subsequent thermal load without major change in optical properties or residual stress.

ACKNOWLEDGMENTS

This work was carried out within the MECHALD project funded by Business Finland and is linked to the Finnish Centers of Excellence in Atomic Layer Deposition (Ref. No. 251220) and Nuclear and Accelerator Based Physics (Ref Nos. 213503 and 251353) of the Academy of Finland.

AUTHOR DECLARATIONS

Conflict of Interest

The authors have no conflicts to disclose.

Author Contributions

O.Y. designed the experiments with A.L. and R.L.P. O.Y. fabricated thermal $\text{Me}_3\text{Al-H}_2\text{O}$ samples at a temperature range from 110 to 300 °C and made thickness and residual stress characterization and thermal annealing and cycling and related data analysis under supervision of R.L.P. A.L. made refractive index and extinction coefficient measurements on a wavelength range from 190 to 1645 nm. S.E. fabricated samples with thermal $\text{Me}_3\text{Al-O}_3$ and plasma $\text{Me}_3\text{Al-O}_2$ processes. J.M. fabricated thermal $\text{Me}_3\text{Al-H}_2\text{O}$ samples at a temperature range from 30 to 110 °C. J.J. and M.L. performed the ToF-ERDA measurements and the analysis under the supervision of T.S. S.A. and S.S. made the XRR and GIXRD measurements and the data analysis under supervision of H.L. Project management, supervision, and resource management were done by R.L.P. O.Y. did writing of the original draft and editing of the review. All authors discussed the results and commented the manuscript by O.Y.

Oili M. E. Ylivaara: Conceptualization (equal); Data curation (lead); Formal analysis (lead); Writing – original draft (lead);

Writing – review & editing (lead). **Andreas Langner:** Conceptualization (equal); Data curation (supporting); Formal analysis (supporting); Writing – review & editing (supporting). **Satu Ek:** Data curation (supporting); Writing – review & editing (supporting). **Jari Malm:** Data curation (supporting); Formal analysis (supporting); Writing – review & editing (supporting). **Jaakko Julin:** Data curation (supporting); Formal analysis (supporting); Writing – review & editing (supporting). **Mikko Laitinen:** Data curation (supporting); Formal analysis (supporting); Writing – review & editing (supporting). **Saima Ali:** Data curation (supporting); Formal analysis (supporting); Writing – review & editing (supporting). **Sakari Sintonen:** Data curation (supporting); Formal analysis (supporting); Writing – review & editing (supporting). **Harri Lipsanen:** Supervision (supporting); Writing – review & editing (supporting). **Timo Sajavaara:** Supervision (supporting); Writing – review & editing (supporting). **Riikka L. Puurunen:** Conceptualization (equal); Formal analysis (supporting); Funding acquisition (lead); Supervision (lead); Writing – review & editing (equal).

DATA AVAILABILITY

The data that support the findings of this study are openly available in Zenodo at <http://doi.org/10.5281/zenodo.7105571>, Ref. 73. The data that support the findings of this study are available from the corresponding author upon reasonable request.

REFERENCES

- 1 M. Leskelä and M. Ritala, *Thin Solid Films* **409**, 138 (2002).
- 2 O. Sneh, R. B. Clark-Phelps, A. R. Londergan, J. Winkler, and T. E. Seidel, *Thin Solid Films* **402**, 248 (2002).
- 3 R. L. Puurunen, *J. Appl. Phys.* **97**, 121301 (2005).
- 4 S. M. George, *Chem. Rev.* **110**, 111 (2010).
- 5 V. Miikkulainen, M. Leskelä, M. Ritala, and R. L. Puurunen, *J. Appl. Phys.* **113**, 021301 (2013).
- 6 G. N. Parsons *et al.*, *J. Vac. Sci. Technol. A* **31**, 050818 (2013).
- 7 R. L. Puurunen, *Chem. Vap. Depos.* **20**, 332 (2014).
- 8 A. Yanguas-Gil, “Thin film growth in nanostructured materials,” in *Growth and Transport in Nanostructured Materials: Reactive Transport in PVD, CVD, and ALD* (SpringerBriefs in Materials, Springer, Cham, 2017).
- 9 J. R. Van Ommen, A. Goulas, and R. L. Puurunen, “Atomic layer deposition,” *Kirk-Othmer Encyclopedia of Chemical Technology* (John Wiley & Sons, Hoboken, 2021), pp. 1–42.
- 10 N. D. Hoivik, J. W. Elam, R. J. Linderman, V. M. Bright, S. M. George, and Y. C. Lee, *Sens. Actuators, A* **103**, 100 (2003).
- 11 R. L. Puurunen, J. Saarihahti, and H. Kattelus, *ECS Trans.* **11**, 3 (2007).
- 12 R. L. Puurunen *et al.*, *Sens. Actuators, A* **188**, 240 (2012).
- 13 M. F. Doerner and W. D. Nix, *Crit. Rev. Solid State Mater. Sci.* **14**, 225 (1988).
- 14 W. D. Nix, *Metall. Trans. A* **20**, 2217 (1989).
- 15 J. A. Thornton and D. W. Hoffman, *Thin Solid Films* **171**, 5 (1989).
- 16 P. J. Withers and H. K. D. H. Bhadeshia, *Mater. Sci. Technol.* **17**, 366 (2001).
- 17 W. S. Yang, Y. K. Kim, S.-Y. Yang, J. H. Choi, H. S. Park, S. I. Lee, and J.-B. Yoo, *Surf. Coat. Technol.* **131**, 79 (2000).
- 18 G. Krauthelm, T. Hecht, S. Jakschik, U. Schröder, and W. Zahn, *Appl. Surf. Sci.* **252**, 200 (2005).
- 19 M. K. Tripp, C. Stampfer, D. C. Miller, T. Helbling, C. F. Herrmann, C. Hierold, K. Gall, S. M. George, and V. M. Bright, *Sens. Actuators, A* **130–131**, 419 (2006).
- 20 Y.-J. Chang, J. M. Gray, A. Imtiaz, D. Seghete, T. Mitch Wallis, S. M. George, P. Kabos, C. T. Rogers, and V. M. Bright, *Sens. Actuators, A* **154**, 229 (2009).

- ²¹D. C. Miller, R. R. Foster, S.-H. Jen, J. A. Bertrand, S. J. Cunningham, A. S. Morris, Y.-C. Lee, S. M. George, and M. L. Dunn, *Sens. Actuators, A* **164**, 58 (2010).
- ²²B. Vermang, H. Goverde, V. Simons, I. De Wolf, J. Meersschart, S. Tanaka, J. John, J. Poortmans, and R. Mertens, in *2012 38th IEEE Photovoltaic Specialists Conference* in Austin, TX, USA, 03-08 June 2012 (IEEE, Austin, TX, 2012), pp. 001135–001138.
- ²³J. P. Colonna *et al.*, *J. Vac. Sci. Technol. B* **29**, 01AE02 (2011).
- ²⁴J. Maula, K. Härkönen, and A. Nikolov, U.S. patent US00,790,173,6B2 (8 March 2011).
- ²⁵R. E. Sah, R. Driad, F. Bernhardt, L. Kirste, C.-C. Leancu, H. Czap, F. Benkhelifa, M. Mikulla, and O. Ambacher, *J. Vac. Sci. Technol. A* **31**, 041502 (2013).
- ²⁶R. E. Sah, C. Tegenkamp, M. Baeumlner, F. Bernhardt, R. Driad, M. Mikulla, and O. Ambacher, *J. Vac. Sci. Technol. B* **31**, 04D111 (2013).
- ²⁷H. B. Profijt, M. C. M. Van De Sanden, and W. M. M. Kessels, *J. Vac. Sci. Technol. A* **31**, 01A106 (2013).
- ²⁸O. M. E. Ylivaara *et al.*, *Thin Solid Films* **552**, 124 (2014).
- ²⁹T. Süss, P. Braeuninger-Weimer, and C. Hierold, *Sens. Actuators, A* **212**, 159 (2014).
- ³⁰M. Berdova *et al.*, *Acta Mater.* **66**, 370 (2014).
- ³¹M. Berdova *et al.*, *Nanotechnology* **25**, 355701 (2014).
- ³²A. Bulusu, A. Singh, C. Y. Wang, A. Dindar, C. Fuentes-Hernandez, H. Kim, D. Cullen, B. Kippelen, and S. Graham, *J. Appl. Phys.* **118**, 085501 (2015).
- ³³A. Behrendt, J. Meyer, P. Van De Weijer, T. Gahlmann, R. Heiderhoff, and T. Riedl, *ACS Appl. Mater. Interfaces* **8**, 4056 (2016).
- ³⁴O. M. E. Ylivaara *et al.*, *J. Vac. Sci. Technol. A* **35**, 01B105 (2017).
- ³⁵S. Shestaeva, A. Bingel, P. Munzert, L. Ghazaryan, C. Patzig, A. Tunnermann, and A. Szeghalmi, *Appl. Opt.* **56**, C47 (2017).
- ³⁶Z. Zhu, E. Salmi, and S. Virtanen, in *2017 IEEE 12th International Conference on ASIC (ASICON)*, Guiyang, Peoples R. China, Oct. 25-28, 2017. WOS: 000426983400059, pp. 233–236.
- ³⁷J. T. Gaskins *et al.*, *ECS J. Solid State Sci. Technol.* **6**, N189 (2017).
- ³⁸M. Broas, H. Jiang, A. Graff, T. Sajavaara, V. Vuorinen, and M. Paulasto-Kröckel, *Appl. Phys. Lett.* **111**, 141606 (2017).
- ³⁹V. Prodanovic, H. W. Chan, H. V. D. Graaf, and P. M. Sarro, *Nanotechnology* **29**, 155703 (2018).
- ⁴⁰V. Rontu, A. Nolvi, A. Hokkanen, E. Haegström, I. Kassamakov, and S. Franssila, *Mater. Res. Express* **5**, 046411 (2018).
- ⁴¹V. Beladiya, T. Faraz, W. M. M. Kessels, A. Tünnermann, and A. Szeghalmi, *Proc. SPIE* **10691**, 106910E (2018).
- ⁴²A. Lale, E. Scheid, F. Cristiano, L. Datas, B. Reig, J. Launay, and P. Temple-Boyer, *Thin Solid Films* **666**, 20 (2018).
- ⁴³Z. Zhu, S. Merdes, O. M. E. Ylivaara, K. Mizohata, M. J. Heikkilä, and H. Savin, *Phys. Status Solidi A* **217**, 1900237 (2020).
- ⁴⁴L. Ghazaryan, S. Handa, P. Schmitt, V. Beladiya, V. Roddatis, A. Tunnermann, and A. Szeghalmi, *Nanotechnology* **32**, 095709 (2021).
- ⁴⁵M. Gebhard *et al.*, *ACS Appl. Mater. Interfaces* **10**, 7422 (2018).
- ⁴⁶E. Sortino, J. P. Houlton, J. C. Gertsch, O. D. Supekar, G. D. Skidmore, S. M. George, C. T. Rogers, and V. M. Bright, *2019 20th International Conference on Solid-State Sensors, Actuators and Microsystems & Eurosensors XXXIII (TRANSDUCERS & EUROSensors XXXIII)* (IEEE, 2019), pp. 2404–2407.
- ⁴⁷S. H. Jen, S. M. George, R. S. Mclean, and P. F. Carcia, *ACS Appl. Mater. Interfaces* **5**, 1165 (2013).
- ⁴⁸J. S. Park, S. H. Yong, Y. J. Choi, and H. Chae, *AIP Adv.* **8**, 085101 (2018).
- ⁴⁹A. K. Sinha, H. J. Levinstein, and T. E. Smith, *J. Appl. Phys.* **49**, 2423 (1978).
- ⁵⁰J. Thurn and M. P. Hughey, *J. Appl. Phys.* **95**, 7892 (2004).
- ⁵¹J. Thurn and R. F. Cook, *J. Mater. Sci.* **39**, 4799 (2004).
- ⁵²O. M. E. Ylivaara *et al.*, *Thin Solid Films* **732**, 138758 (2021).
- ⁵³R. Raghavan, M. Bechelany, M. Parlinska, D. Frey, W. M. Mook, A. Beyer, J. Michler, and I. Utke, *Appl. Phys. Lett.* **100**, 191912 (2012).
- ⁵⁴L. Hennen, E. H. A. Granneman, and W. M. M. Kessels, in *2012 38th IEEE Photovoltaic Specialists Conference*, 03-08 June, Austin, TX, USA (IEEE, Austin, TX, 2012), pp. 001049–001054.
- ⁵⁵S. Li, P. Repo, G. Von Gastrow, Y. Bao, and H. Savin, in *2013 IEEE 39th Photovoltaic Specialists Conference (PVSC)*, 16-21 June 2013, Tampa, FL, USA (IEEE, 2013), pp. 1265–1267.
- ⁵⁶A. Werbrouck, K. Van De Kerckhove, D. Depla, D. Poelman, P. F. Smet, J. Dendooven, and C. Detavernier, *J. Vac. Sci. Technol. A* **39**, 062402 (2021).
- ⁵⁷E. Beche *et al.*, *ECS J. Solid State Sci. Technol.* **4**, P171 (2015).
- ⁵⁸S. Zhao, G. Yuan, D. Zhang, P. Xu, G. Li, and W. Han, *J. Mater. Sci.* **56**, 17478 (2021).
- ⁵⁹D. R. G. Mitchell, D. J. Attard, K. S. Finnie, G. Triani, C. J. Barbé, C. Depagne, and J. R. Bartlett, *Appl. Surf. Sci.* **243**, 265 (2005).
- ⁶⁰B. Nalcaci and M. Polat Gonullu, *Appl. Phys. A* **127**, 460 (2021).
- ⁶¹O. M. E. Ylivaara *et al.*, in *Poster presentation at AVS ALD 2014* (14th International Conference on Atomic Layer Deposition), June 15-18, 2014, Kyoto, Japan.
- ⁶²M. L. Grilli, D. Valerini, A. Rizzo, M. Yilmaz, C. Song, G. H. Hu, A. Mikhaylov, R. Chierchia, and A. Rinaldi, *Phys. Status Solidi A* **219**, 2100398 (2022).
- ⁶³I. Reklaitis *et al.*, *Surf. Coat. Technol.* **399**, 126123 (2020).
- ⁶⁴M. Laitinen, M. Rossi, J. Julin, and T. Sajavaara, *Nucl. Instrum. Methods Phys. Res. Sect. B* **337**, 55 (2014).
- ⁶⁵K. Arstila *et al.*, *Nucl. Instrum. Methods Phys. Res. Sect. B* **331**, 34 (2014).
- ⁶⁶(2022).
- ⁶⁷S. Jakschik, U. Schroeder, T. Hecht, M. Gutsche, H. Seidl, and J. W. Bartha, *Thin Solid Films* **425**, 216 (2003).
- ⁶⁸K. Y. Gao, F. Speck, K. Emtsev, T. Seyller, and L. Ley, *J. Appl. Phys.* **102**, 094503 (2007).
- ⁶⁹J. M. Rafi, M. Zabala, O. Beldarrain, and F. Campabadal, *J. Electrochem. Soc.* **158**, G108 (2011).
- ⁷⁰L. Nistor, O. Richard, C. Zhao, H. Bender, A. Stesmans, and G. Van Tendeloo, *Inst. Phys. Conf. Ser.* **180**, 397 (2003).
- ⁷¹L. Zhang, H. C. Jiang, C. Liu, J. W. Dong, and P. Chow, *J. Phys. D: Appl. Phys.* **40**, 3707 (2007).
- ⁷²D. York, *Earth Planet. Sci. Lett.* **5**, 320 (1968).
- ⁷³See <http://doi.org/10.5281/zenodo.7105571> for supplementary dataset for ALD thermal cycling.